Available online at www.sciencedirect.com
SCIENCE DIRECT®
ELSEVIER
Journal of Magnetism and Magnetic Materials 293 (2005) 647–654
Journal of magnetism and magnetic materials
www.elsevier.com/locate/jmmm

Targeted drug delivery to magnetic implants for therapeutic applications

Benjamin B. Yellen[a,*], Zachary G. Forbes[b], Derek S. Halverson[a], Gregory Fridman[b], Kenneth A. Barbee[a,b], Michael Chorny[c], Robert Levy[c], Gary Friedman[a,b]

[a]*Electrical & Computer Engineering Department, Drexel University, 3141 Chestnut Street, Philadelphia, PA 19104, USA*
[b]*Drexel University School of Biomedical Engineering and Health Sciences, Philadelphia, PA 19104, USA*
[c]*The Children's Hospital of Philadelphia and The University of Pennsylvania, School of Medicine, Philadelphia, PA 19104, USA*

Available online 5 March 2005

Abstract

A new method for locally targeted drug delivery is proposed that employs magnetic implants placed directly in the cardiovascular system to attract injected magnetic carriers. Theoretical simulations and experimental results support the assumption that using magnetic implants in combination with externally applied magnetic field will optimize the delivery of magnetic drug to selected sites within a subject.

PACS: 47.65.+a; 47.85.−g; 75.50.Mm; 75.50.−y; 75.50.Tt; 75.50.Ww; 87.68.+z; 87.80.−y

Keywords: Drug delivery; Stent; Magnetic implant; Local drug delivery; Targeted; Implant

The ability to safely and effectively deliver high dosages of drugs to specific sites in the human body is fundamental to the advancement of drug delivery based therapeutic strategies. Drugs with proven effectiveness under in vitro investigation often reach a major roadblock during in vivo testing due to a lack of an effective delivery strategy. In addition, many clinical scenarios require delivery of agents that are therapeutic at the desired delivery point but otherwise systemically toxic. Thus the ability to adequately localize injected drug is paramount to an effective drug delivery strategy.

Magnetic fields based delivery schemes are one of the most attractive methods for localizing drug in the body, because magnetic forces act at relatively long range and magnetic fields do not affect most biological tissues. Methods and devices proposed in the past to deliver drugs encapsulated within magnetic carriers to specific locations in the

*Corresponding author. Tel.: +1 215 895 0271; fax: +1 215 895 0280.
E-mail address: yellen@email.chop.edu (B.B. Yellen).

0304-8853/$ - see front matter © 2005 Published by Elsevier B.V.
doi:10.1016/j.jmmm.2005.01.083

body have relied on a single source of magnetic field, both to magnetize the carriers and to pull them by magnetic force to specified locations in the body [1–6]. These single magnetic field sources are usually applied either externally to the body or through the use of an internal implant. However, this single source capture method is at odds with the underlying physical mechanism of magnetic particle capture, which depends on the presence of both strong far-reaching magnetic fields to magnetize the carriers and strong magnetic field gradients to apply forces on those carriers. On the one hand, sources applied external to the body are excellent for magnetizing the carriers, but they provide only weak magnetic field gradients to attract them. On the other hand, an internal magnetic implant provides strong magnetic field gradients to attract the carriers, but its fields decay too quickly to magnetize the bulk of the injected carriers.

In this paper, a new method for locally targeted drug delivery based on the use of two independent magnetic sources is proposed. This magnetic drug delivery system is novel in that the steps of magnetizing the carriers and providing the magnetic field gradients to capture the carriers are accomplished separately through the use of micron-sized magnetic implants in combination with long-range externally applied magnetic fields [7]. This system can potentially optimize the capture and localization of carriers at desired sites in the body. This problem has been studied both theoretically and experimentally, and in vitro experimental results have shown that it is possible to capture high concentrations of even sub-micron sized magnetic carriers at selected sites, which is of great interest to clinicians in the field.

Similar theoretical and experimental work on the attraction of magnetic materials onto small ferromagnetic wires and spheres in flow has been performed by Friedlaender et al. [8–13]. Although the basic theory and experimental setup is quite similar to the work presented in this paper, Friedlaender's group studied the separation of larger and more strongly magnetic particles for applications in filtering of waste materials. The magnetic interactions between such large magnetic particles could lead to significant particle clumping and considerable adverse side-effects if used in the cardiovascular system. By contrast, the work performed in this paper has focused on the use of biocompatible, superparamagnetic particles which are less magnetically responsive but more suitable for use in clinical applications.

Computational analysis, performed using MATHCAD software, focused on ascertaining the feasibility of capturing particles with magnetic implants in the presence of other competing forces. In these systems, the particle's mass is so small that gravity can be neglected, so the main competition against the magnetic force is hydrodynamic drag. Experiments in this work have used a wire mesh that was electroplated with Co/Ni alloy to produce the localized magnetic field gradients. The mesh was placed in direct contact with the fluid in order to simulate the conditions produced by a magnetic stent implanted in the cardiovascular system. With the aid of magnetic measurements on the electroplated mesh performed by an alternating gradient magnetometer (AGM) at Princeton Measurements Corporation (Princeton, NJ), theoretical models have attempted to describe the system of magnetic particle capture in order to guide current and future experiments.

To simplify models, the mesh was approximated as a planar 3×3 array of magnetic wires, as shown in Fig. 1. This assumption is quite reasonable since the magnetic carriers will only feel the magnetic gradients of the closest few wires in the implant. The wires are assumed to be uniformly magnetized perpendicularly to their long axes by externally produced uniform magnetic fields. These assumptions allow for an analytical solution for each wire's magnetic scalar potential to be obtained [14]. This potential is given by the following expression:

$$\varphi_{\text{wire}}(\vec{r},\theta) = \frac{\vec{\lambda}_{\text{wire}}}{2\pi}\frac{\cos(\theta)}{\vec{r}}. \quad (1)$$

The magnetic moment per unit length of the wire is denoted by λ_{wire} where $\vec{r}$ is a vector of magnitude, $|r|$, at an angle θ with the applied magnetic field. The measured magnetic moment per unit length of the wire was found to relate linearly with the applied field $\vec{H}_0$ in the range of 0–300 G, as $\vec{\lambda}_{\text{wire}} = \vec{H}_0 \cdot (1.3 \times 10^{-6}\,\text{m}^2) + 6.8 \times 10^{-5}\,\text{A m}$, as can be

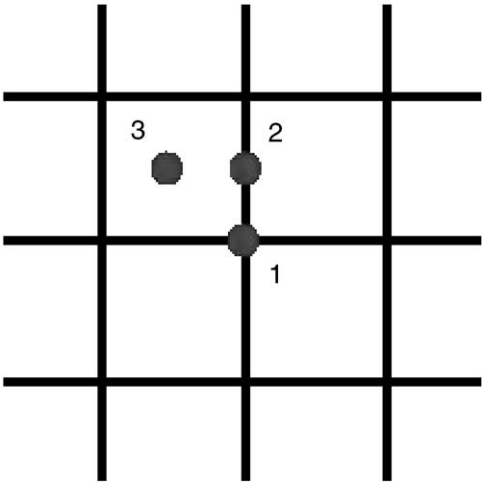

Fig. 1. Simplified version of a magnetic mesh, consisting of a 3×3 array of magnetic wires. The spots labeled 1, 2, and 3, indicate the starting positions the magnetic force profiles taken in theoretical simulations.

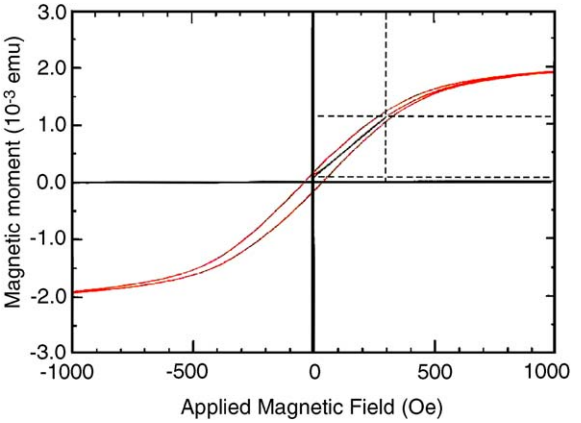

Fig. 2. Major hysteresis loop and a reversal curve measured starting from the upper portion of the major loop for the CoNi plated wire. Measurement was performed with Princeton Measurement Corp., Alternating Gradient Force Magnetometer.

seen from the hysteresis curve originating from the upper hysteresis branch in Fig. 2. Using the magnetic scalar potential, the magnetic fields produced by the wires can be computed by taking its gradient.

Once the magnetic fields in the system are known, it is possible to calculate the magnetic moments of the carriers and the magnetic forces applied to them. All magnetic carriers are considered to be superparamagnetic beads that are uniformly magnetized, which is a reasonable approximation for non-interacting beads. In the case of a linear relationship between magnetization and magnetic field, the bead's magnetic moment is given by

$$\vec{m} = \chi V \vec{H}, \tag{2}$$

where $\chi \approx 2.5$ is the effective bead susceptibility as measured by AGM, and V is the volume of the spherical bead. Using the dipole moment calculated by the applied magnetic fields, the force on the bead can be determined according to

$$\vec{F}_{\text{mag}} = \mu_0(\vec{m} \cdot \nabla)\vec{H}. \tag{3}$$

The horizontal drag on each particle of radius a in a fluid of viscosity η is given as a function of the velocity $\vec{v}$ of the bulk fluid by

$$\vec{F}_{\text{drag}} = 6\pi\eta a \vec{v}\,. \tag{4}$$

The velocity was assumed to be 15 cm/s to approximate the flow conditions in the coronary artery.

Using these equations, the ratio of the magnetic to hydrodynamic force on the beads was computed to ascertain if the magnetic force produced by the mesh can compete with the drag force on the magnetic carriers. This ratio represents only a gross approximation and several interactions are ignored. For example, magnetic interactions between adjacent wires are ignored and the interactions between nearby beads are neglected in the magnetic force calculations. Only the vertical magnetic field and force components were used in simulations. In addition, the hydrodynamic drag neglects wall effects associated with Poiseuille flow by modeling the force as a constant magnitude proportional only to the bulk fluid flow velocity. Under these assumptions, the following magnetic to hydrodynamic force ratio is obtained from (2)–(4):

$$R = \left|\frac{2\chi a^2}{9v\eta}\vec{H} \cdot \nabla\vec{H}\right|. \tag{5}$$

It is believed the above simplified scaling ratio represents the worst case scenario, while still giving a general idea of how the forces scale and if bead capture is possible. From Eq. (5), it is clear that the force ratio scales with the square of the bead's radius. Therefore, it is predicted that larger magnetic beads can be captured more easily, though administration of smaller beads is more desirable from a clinician's perspective. Hence an optimal bead size can be deduced from these equations that still allows for significant capture while minimizing the size of the bead.

Force profiles in the vertical direction were computed for three different starting positions above the mesh, and the results are shown in Figs. 3–5. Fig. 3a and b show the force profiles on a 2 μm bead and on a 370 nm bead respectively, as the bead moves in the vertical direction away from the intersection of two magnetic wires, depicted as starting position (1) in the illustration in Fig. 1. The series of curves in each graph represents the force profiles as a function of uniformly applied magnetic fields set at discrete values between 0 and 300 G in multiples of 50 G. The darkened line in each of the graphs indicates the magnetic field strength of 150 G that was typically used in experimental testing. Fig. 4 shows the same

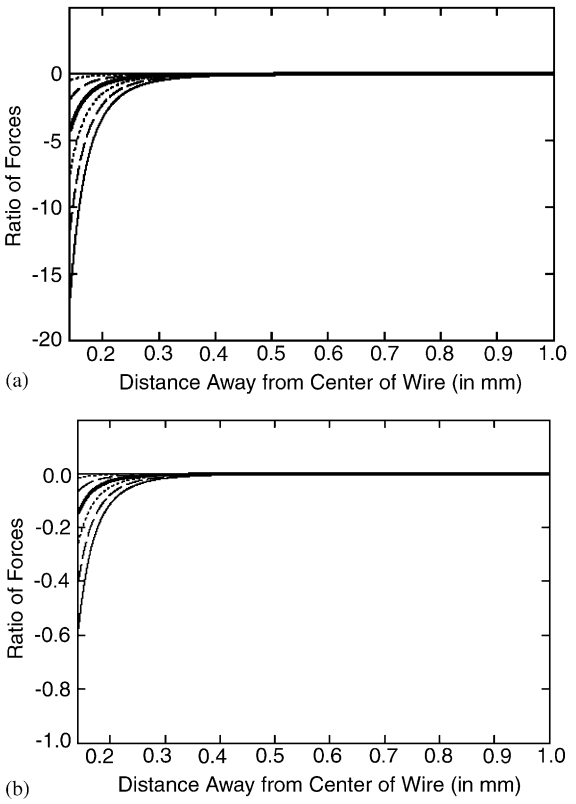

Fig. 3. Force profiles at various applied magnetic fields on (a) 2 μm beads, and (b) 370 nm beads. The series of lines indicate the force profiles taken at applied magnetic field strengths ranging from 0 to 300 G, in multiples of 50 G, on the beads starting at the surface of the intersection of two wires and moving vertically away from the mesh. The darkened line indicates the force profile taken for beads under an applied field of 150 G.

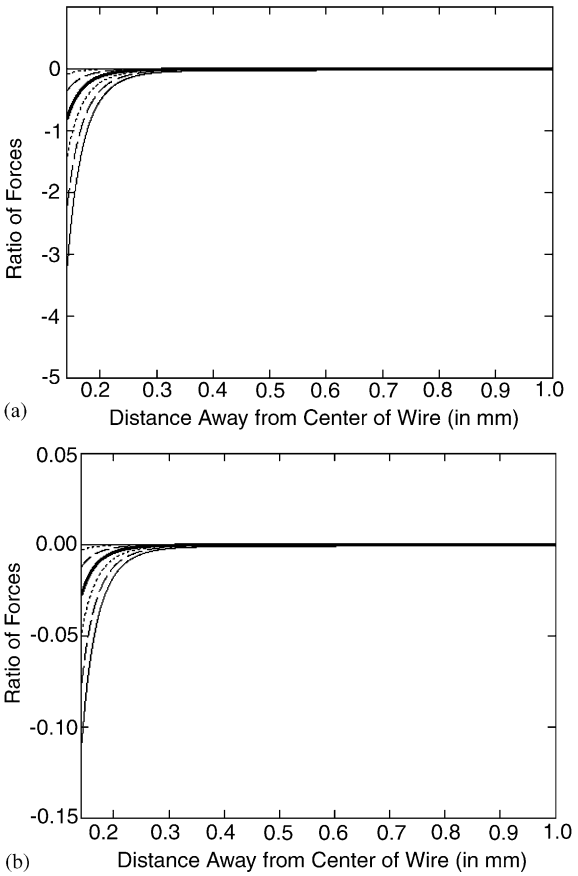

Fig. 4. Force profiles at various applied magnetic fields on (a) 2 μm beads, and (b) 370 nm beads. The series of lines indicate the force profiles taken at applied magnetic field strengths ranging from 0 to 300 G, in multiples of 50 G, on the beads starting at the surface of a single wire and moving vertically away from the mesh. The darkened line indicates the force profile taken for beads under an applied field of 150 G.

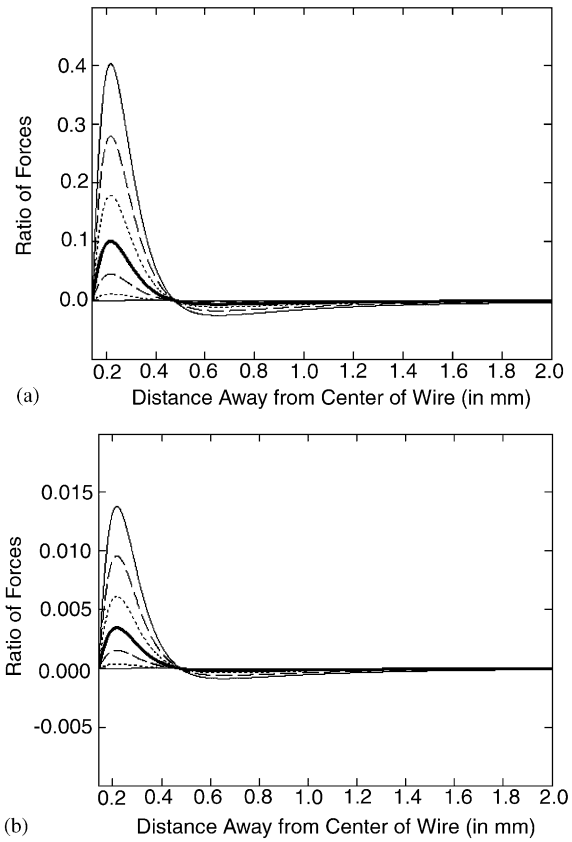

Fig. 5. Force profiles at various applied magnetic fields on (a) 2 μm beads, and (b) 370 nm beads. The series of lines indicate the force profiles taken at applied magnetic field strengths ranging from 0 to 300 G, in multiples of 50 G, on the beads starting at a position in the space between the wires and moving vertically away from the mesh. The darkened line indicates the force profile taken for beads under an applied field of 150 G.

analysis for the beads moving vertically away from the surface of a single wire, which is depicted as starting position (2) in Fig. 1, and Fig. 5 shows the same analysis for a bead moving vertically away from the space in between the wires, which is depicted as starting position (3) in Fig. 1. Negative numbers indicate that the net magnetic force results in attraction towards the mesh, whereas positive numbers indicate a net repulsion away from the mesh.

An image of the wire mesh used in experiments is shown in Fig. 6. The typical mesh wire diameter is roughly 140 μm with a period of approximately

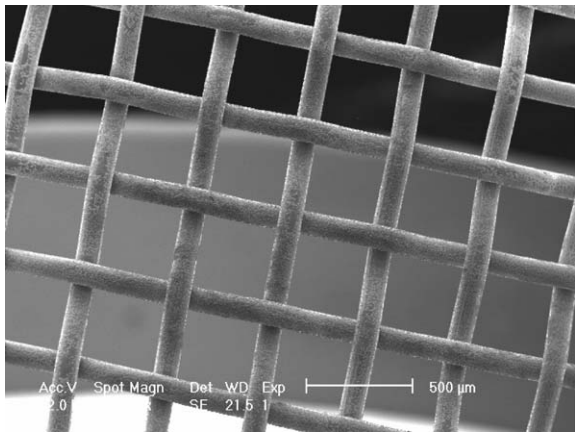

Fig. 6. SEM image of the stainless steel mesh electroplated with cobalt–nickel alloy that was the sole source of magnetic field gradients in experiments.

500 μm in between adjacent wires. These mesh parameters were used in the simulations shown graphically in Figs. 3–5. The viscosity of water was used in these simulations. Results led us to believe that only the beads in the vicinity of a few wire diameters from the mesh would be caught, whereas the majority of beads would escape. Even though most material according to simulations would not be captured, the local accumulation of beads on the mesh can still be quite high. Since the number of injected beads would be considered a low dose for the human body as a whole, this capture method is consistent with the goal of delivering a high dose of therapeutic agents to locally targeted sites without administering systemically toxic dosages.

According to these results, the magnetic beads are most strongly attracted to the intersection of wires shown in Fig. 3, since these regions produce the strongest magnetic field gradients. Results also predict that magnetic beads are only weakly attracted to, and in some cases even repelled from, the space in between the mesh struts as shown in Fig. 5. As expected, simulations predict that large 2 μm beads are more easily captured by the mesh than 370 nm beads, since the ratio of magnetic to hydrodynamic force should scale with the square of the bead's radius. Based on these simulations, significant capture of only the 2 μm beads was anticipated.

Experiments were performed with a magnetic mesh that was electroplated with Co/Ni alloy by electrodeposition techniques described previously in the literature [15–17]. The electrodeposited material was chosen to combine the strong magnetic properties of Cobalt with the plating uniformity of Nickel. Additives such as Saccharin and NaCl were employed to reduce the stress on the plated material. By measuring the sample weight before and after material deposition, it was estimated that a 5 μm thick coating was deposited onto the mesh.

A 2 cm × 2 cm piece of mesh was fixed inside a parallel plate flow chamber with a flow cross-section measuring 27 mm wide by 2.5 mm tall. The goal in designing the pattern dimensions and flow environment was to simulate an 'unrolled' stent, with the height of the channel being roughly the radius of the coronary artery. The flow chamber was then mounted on a microscope stand, and external uniform magnetic fields of 150 G were applied to the flow chamber in the vertical direction during flow experiments so that particle capture could be visualized in real-time. Magnetic fields were produced by passing current through a solenoid coil with iron core placed underneath the flow chamber. The magnetic field strength was measured by a Hall Probe purchased from Lake Shore Cyrotronics (Westerville, OH).

Two different particle types were used in experiments. Particles used in the first flow experiments were commercially available superparamagnetic polystyrene beads purchased from Spherotech (Libertyville, IL). These beads, composed of 20% γ-Fe_2O_3 magnetite by weight and labeled with red fluorescent pigment, had a nominal diameter of 2 μm with approximately 10% variance in size. In the second set of experiments, a proprietary method was used to prepare fluorescent-labeled (BODIPY 564/570) biodegradable polylactic acid-based particles loaded with magnetite. This population of nanoparticles had an average diameter of 370 nm with a size distribution spanning the range of 364–382 nm. These nanoparticles were found to have similar magnetic material properties ($\chi \approx 2.5$) as the commercially available beads from Spherotech.

In these experiments, 10^8 beads of 2 μm diameter or 10^{12} beads of 370 nm diameter, each suspended in 10 ml of solution, were flown into the flow chamber at an average velocity of 5 cm/s in a single pass followed by thorough rinsing with saline solution. Afterwards, the mesh was visually inspected with a Leica LM-DFS fluorescent microscope in order to determine the efficiency of particle capture. As a control, these experiments were also performed with non-magnetic mesh and the results are shown in comparison in Figs. 7 and 8. As demonstrated by Fig. 7, significant

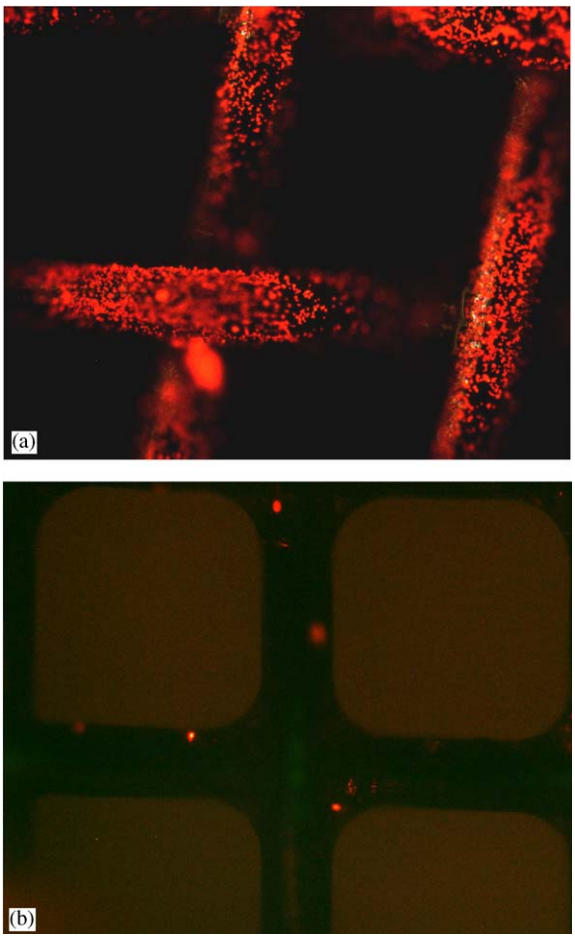

Fig. 7. Capture of 2 μm magnetic particles on (a) electroplated magnetic mesh and (b) non-magnetic mesh, in 5 cm/s flow velocity inside a parallel plate flow chamber. Bead capture on the magnetic mesh shows strong accumulation of particles at the edge of the mesh, whereas little or no capture was observed on the non-magnetic mesh.

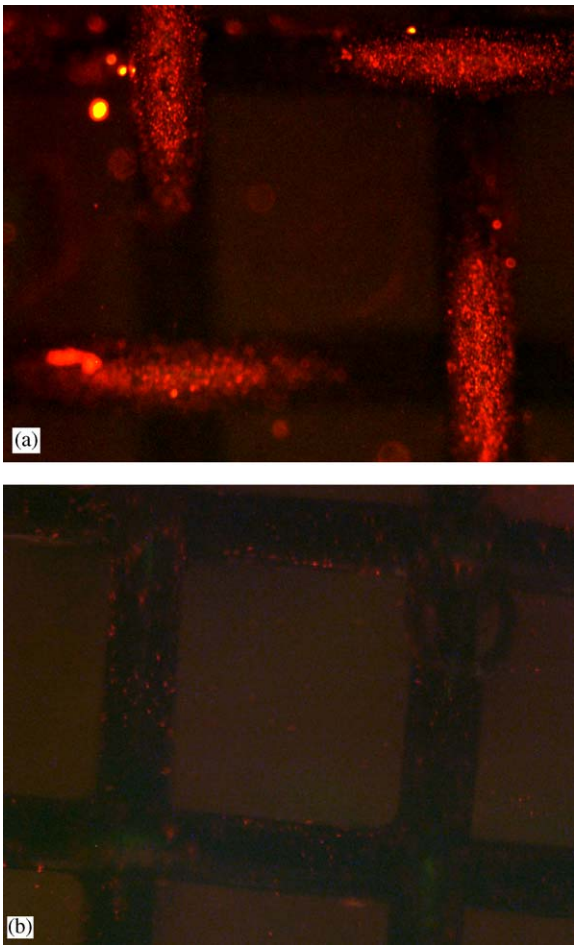

Fig. 8. Capture of 370 nm magnetic particles on (a) electroplated magnetic mesh and (b) non-magnetic mesh, in 5 cm/s flow velocity inside a parallel plate flow chamber. Bead capture on the magnetic mesh shows strong accumulation of particles at the edge of the mesh, whereas little or no capture was observed on the non-magnetic mesh.

capture of the 2 μm diameter beads was achieved by the magnetic mesh, while relatively low bead capture was achieved by the non-magnetic mesh. These results are consistent with theoretical models describing the physics of particle capture. Not surprisingly, the largest concentration of captured particles was located at the intersections between the magnetic wires where the magnetic field gradients are expected to be maximal.

We were surprised to find, however, that 370 nm beads were also capable of being captured by the magnetic mesh, as demonstrated in Fig. 8. Models predicted that the magnetic force at the surface of the mesh near the intersection of two wires would be approximately 1/10 of the hydrodynamic drag force, which means that the fluid forces would overpower the magnetic attraction of these beads to the mesh. It was mentioned previously that these models represented the lower limit of our estimates. Poiseuille flow profiles predict that the fluid velocity near the walls of a channel should be significantly weaker than near the center of the channel. The fluid velocity near the mesh could be an order of magnitude weaker than in bulk flow, which would explain why beads were captured even though simulations predicted otherwise. Again, bead capture occurred primarily near the intersections between wires in the mesh, which is consistent with theoretical simulations.

In conclusion, locally targeted drug delivery using two magnetic sources was theoretically modeled and experimentally demonstrated as a new method for optimizing the delivery of magnetic carriers in high concentration to specific sites in the human body. Theoretical models predict that the externally applied magnetic fields have a pronounced effect on particle capture. Theory suggests that for clinical applications, magnetic fields in the range of 0.1 T should be used so that both the particles and the implant are magnetized to the point of saturation. Fields greater than 0.1 T will have little additional effect on bead capture. Experimental results have demonstrated that capturing superparamagnetic beads of both micrometer and sub-micrometer diameter at reasonably high concentrations is possible in flow conditions consistent with the dimensions and flow velocity occurring in the coronary artery in the human body. The same experiments performed with non-magnetic mesh resulted in no significant capture, indicating that the implant is responsible for providing the necessary magnetic field gradients and forces to capture the injected beads.

This work was supported in part by the National Science Foundation under Grant NSF 9984276 and a research grant from the Nanotechnology Institute. Dr. Levy's efforts were supported

in part by the William J. Rashkind Endowment of the Children's Hospital of Philadelphia. The authors are grateful to Anthony Cumbo and Harry Reichard for their help in performing the magnetic measurements on the magnetic particles and magnetic mesh.

References

[1] K. Mossbach, U. Schroder, FEBS Lett. 102 (1979) 112.
[2] J.M. Gallo, U. Häfeli, Corr. re: A.S. Lübbe, et al., Cancer Res. 57 (1997) 3063.
[3] A.S. Lübbe, C. Alexiou, C. Bergemann, J. Surg. Res. 95 (2001) 200.
[4] S. Rudge, C. Peterson, C. Vessely, et al., J. Contr. Release 74 (2001) 335.
[5] G.A. Flores, Eur. Cells Mater. 3 (2002) 9.
[6] P.A. Voltairas, D.I. Fotiadis, L.K. Michalis, 35 (2002) 813.
[7] Z.G. Forbes, B.B. Yellen, K.A. Barbee, et al., IEEE Trans. Magn. 39 (2003) 3372.
[8] W. Leitermann, F.J. Friedlaender, R. Gerber, et al., IEEE Trans. Magn. 20 (1984) 1174.
[9] F.J. Friedlaender, M. Takayasu, IEEE Trans. Magn. 18 (1982) 817.
[10] C. Cowen, F.J. Friedlaender, R. Jaluria, IEEE Trans. Magn. 11 (1975) 1600.
[11] F.J. Friedlaender, R. Gerber, W. Kurzl, et al., IEEE Trans. Magn. 17 (1981) 2801.
[12] F.J. Friedlaender, R. Gerber, H.P. Henkel, et al., IEEE Trans. Magn. 17 (1981) 2804.
[13] H. Schewe, M. Takayasu, F.J. Friedlaender, IEEE Trans. Magn. 16 (1980) 149.
[14] W. Panofsky, M. Phillips, Classical Electricity and Magnetism, Addison-Wesley, Reading, MA, 1955.
[15] F.A. Lowenheim, Modern Electroplating, McGraw-Hill, New York, 1974.
[16] M. Duch, J. Micromech. Microeng. 12 (2002) 400.
[17] N.V. Myung, et al., Proc. Electrochem. Soc. PV (2000) 506.